

PUBLICATIONS OF  
THE DAVID DUNLAP OBSERVATORY  
UNIVERSITY OF TORONTO

VOLUME II

NUMBER 10

PHOTOELECTRIC  
SPECTROPHOTOMETRY  
OF  
GLOBULAR CLUSTERS

SIDNEY VAN DEN BERGH  
AND  
R. C. HENRY

1962  
TORONTO, CANADA

PRINTED AT  
THE UNIVERSITY OF TORONTO PRESS

# PHOTOELECTRIC SPECTROPHOTOMETRY OF GLOBULAR CLUSTERS

BY SIDNEY VAN DEN BERGH AND R. C. HENRY

## ABSTRACT

A spectrum scanner attached to the 74-inch telescope has been used to derive absolute energy distributions over the range  $\lambda\lambda 3400$  to  $5200$  for the following globular clusters:

NGC 5024 (M53)	NGC 6273 (M19)	NGC 6838 (M71)
NGC 5272 (M3)	NGC 6341 (M92)	NGC 6864 (M75)
NGC 5904 (M5)	NGC 6356	NGC 6934
NGC 6093 (M80)	NGC 6402 (M14)	NGC 7006
NGC 6205 (M13)	NGC 6626 (M28)	NGC 7078 (M15)
NGC 6229	NGC 6656 (M22)	NGC 7089 (M2)
NGC 6254 (M10)	NGC 6779 (M56)	NGC 7099 (M30)

An effective resolution of about  $35\text{\AA}$ . was used for all globular-cluster observations. For comparison purposes the nuclei of the galaxies M31 and M32 and a number of MK standard stars were also observed with the same resolution.

Certain combinations of monochromatic colour indices are found to yield reddening-free parameters which correlate well with Morgan's metallic line strength classification of globular clusters. A discontinuity in the spectral energy distribution near  $\lambda 4000$  is found to correlate with metallic line strength in globular clusters and with metal abundance in main sequence stars. Colour-colour diagrams may be constructed which permit a clear-cut segregation of the effects of interstellar reddening from those of intrinsic colour differences. Observations of M31 show that cyanogen giants provide a major contribution to the total luminosity of the nucleus in blue light.

## INTRODUCTION

THE properties of the integrated light of globular clusters have been studied on low dispersion spectra by Mayall (1946), Morgan (1956, 1959) and Kinman (1959). These investigations have established that globular clusters exhibit a considerable range in spectroscopic characteristics, which may be partially interpreted in terms of differences between the metal abundances of stars in different clusters. Three-colour observations of globular clusters in the galaxy have recently been published by Johnson (1959) and by Kron and Mayall (1960).

It is the purpose of the present investigation to help fill the gap between the very-low-resolution, wide-band photometry and the higher-resolution spectroscopic work. In particular multi-colour

narrow-band photometry should be able to separate the effects of interstellar reddening from intrinsic colour effects. This does not appear to be possible using the wide-band *UBV* and *PVI* systems. Spectral scanning with intermediate resolution also holds promise of being able to measure some of the qualitative differences between globular clusters which have previously been found by visual inspection of cluster spectra.

#### INSTRUMENTATION AND OBSERVING TECHNIQUE

The observations reported in this paper were made with a spectrum scanner designed by J. B. Oke, which is located at the Cassegrain focus of the 74-inch telescope. The light enters the instrument through an entrance diaphragm, which, in the present observing programme, was 4.6 mm. in diameter, corresponding to 28 seconds of arc on the sky. The collimator in the scanner matches the  $f/18$  beam of the telescope and has a focal length of 36 inches. The dispersing element is a Bausch and Lomb replica reflection grating with 600 grooves per millimetre. The centre of its blaze is at  $\lambda 3750$  in the second order, which was the order used. A Newtonian "camera" with a focal length of 9 inches forms an image on an adjustable Hilger spectrograph slit. During the globular cluster observations a slit width of 0.56 millimetres was used, which corresponds to 18.5 A.

Immediately behind the slit is a quartz Fabry lens which has a focal length of 1.4 inches. A selected RCA 1P21 photomultiplier, which was refrigerated by dry ice, was used as a light detector. The output of the photomultiplier was fed to a General Radio 1230 amplifier and recorded by a Brown recorder. During the observations a scanning speed of 4 A./sec. was used, giving a dispersion of 4.6 $\bar{5}$  A./mm. on the tracing. A time constant of 2.5 seconds was employed for all the globular cluster observations. The effective resolution (spectral purity) resulting from the time constant, entrance diaphragm size and exit slit width was about 35A., the exact value depending slightly on the degree of central concentration of light in the globular cluster image.

A single observation consisted of a direct scan from  $\lambda\lambda 5200$  to 3400 and a reverse scan from  $\lambda\lambda 3400$  to 5200 followed, for bright clusters, by a single direct scan of the sky. For those faint clusters, for which the cluster plus sky deflection was less than two or three times larger

than the sky reading, a direct and a reverse sky trace were obtained. Due to the proximity of the city of Toronto to the David Dunlap Observatory the sky background at low altitudes is primarily a function of azimuth. For clusters observed at low altitudes the sky tracings were therefore obtained at the same altitude and azimuth as the cluster tracings. The instrumental arrangement did not permit guiding during the 8 minutes required to make a single scan. For clusters observed near the meridian no serious difficulties due to driving errors, resulting in drifting of the cluster image, were encountered.

DETERMINATION OF THE ATMOSPHERIC ABSORPTION

The following early-type stars, for which Oke (1960) has determined the absolute energy distributions, were used to determine both the atmospheric extinction and the instrumental sensitivity function:

$\xi^2$ Cet B9 III	$\alpha$ CrB A0 V
$\gamma$ Gem A0 IV	$\alpha$ Lyr A0 V
$\alpha$ Leo A B7 V	

The wave-length dependence of the atmospheric extinction was determined by measurements of the same star at high and low altitudes at 12 wave-lengths in the range  $3500 \leq \lambda \leq 5150$  A. (The star  $\alpha$  CrB, which is an eclipsing variable, was not observed at or near times of eclipse.)

TABLE I  
THE OBSERVED ATMOSPHERIC EXTINCTION

$\lambda$	$\lambda^{-1}$ ( $\mu$ )	$K(\lambda) - A$	m.e.
5150	14.22	$0^m.186 \pm 0^m.024$	
5000	16.00	0.204	0.020
4700	20.49	0.227	0.012
4500	24.39	0.256	0.020
4200	32.14	0.358	0.016
4040	37.54	0.412	0.020
3920	42.35	0.461	0.024
3860	45.05	0.474	0.027
3815	47.21	0.471	0.023
3700	53.36	0.593	0.025
3600	59.54	0.684	0.022
3500	66.64	0.743	0.028

It was found that, within the accuracy of the observations, the data for each night could be adequately represented by an equation of the form:

$$K(\lambda) = A + B\lambda^{-4}, \quad (1)$$

in which  $K$  is the absorption (in magnitudes) for one air mass and  $A$  a grey term which varies from night to night. The mean values of  $K(\lambda) - A$ , from 14 extinction observations on 10 nights, are given in Table I and plotted in figure 1. With  $\lambda$  measured in microns a

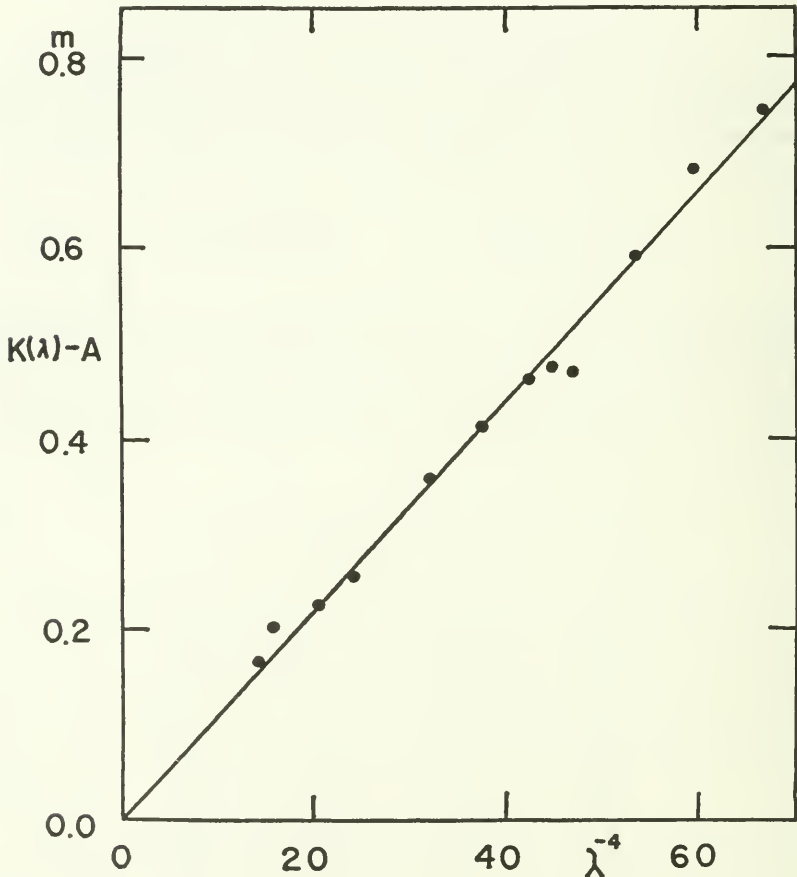


FIG. 1—Wave-length dependence of the atmospheric absorption, with grey term subtracted. The figure shows that the observed absorption may be adequately represented by a  $\lambda^{-4}$  law.

least-squares solution yields the following mean value for the coefficient  $B$  in equation (1):

$$\bar{B} = 0.01085 \pm 0.00021;$$

this may be compared with the value

$$\bar{B} = 0.01077 \pm 0.00017,$$

which Greig (1962) has derived from observations on 12 nights by Bless (1958) at Michigan. (Both Observatories are located at about the same altitude above sea level.)

The value  $B = 0.01085$  was subsequently used for all nights. Actually changes in the atmospheric pressure will result in slight variations of  $B$  from night to night. Use of the mean value of  $B$  will therefore result in random errors, which are, however, judged to be small compared to the observational uncertainty of the determination of  $B$  from observations obtained during a single night. Furthermore not all nights produced a measure of the extinction because on some nights clouds appeared before a second observation of an extinction star could be obtained.

Absorption in the blue and violet region of the spectrum was found to be larger than average on nights during which observations were made through hot moist tropical air. Such nights were characterized by a very red setting sun, a "light" night sky and often by unusually good seeing. Tracings obtained on such nights were not used to derive absolute energy distributions.

#### THE INSTRUMENTAL SENSITIVITY FUNCTION

The observing equipment does not give an identical response when illuminated with equal intensities of light of different wave-lengths. This is due to the wave-length dependence of the reflectivity of the mirrors in the light path and the wave-length dependence of the response of the 1P21 photomultiplier. The instrumental sensitivity function may be determined by comparing the observed spectral energy distribution of Oke's standard stars corrected to outside the atmosphere by means of equation (1), with the absolute energy distributions of these stars which have been published by Oke (1960).

On the average two standard star observations were obtained each night. Usually all individual sensitivity functions obtained during one dark-run were combined into a single mean sensitivity function, which

was then used to reduce all the globular cluster observations obtained during that period.

In deriving the instrumental sensitivity function from observations of Oke's standard stars difficulties were encountered in the region between  $\lambda\lambda 3700$  and  $3900$ . Over this wave-length range the Balmer lines are crowded so close together that limited wave-length resolution, seeing and the amplifier and pen-recorded time constants all tend to lower the observed continuum. In this region Oke therefore recommends the use of a pseudo-continuum drawn through the peaks at a breadth of  $12 \text{ \AA}$ . In our experience this procedure did not yield reproducible results. Since the instrumental sensitivity function changes only slowly with wave-length over this region, a simple interpolation procedure was used. It is believed that the sensitivity function obtained in this way is correct to within  $0^m.02$  at all wave-lengths in the range  $3700 < \lambda < 3900 \text{ \AA}$ .

Extensive data are available on the changes in the instrumental sensitivity function during the period from May 1961 to May 1962 (the mirrors of the 74-inch telescope were re-aluminized in May 1962). Table II summarizes the available data for this period on  $\delta \dot{S}(\lambda)$ , defined as the rate of change of the sensitivity function in magnitudes per year, relative to the rate of change of the sensitivity function at  $\lambda 4500$ . The data in Table II, which are plotted in figure 2, show that the instrumental sensitivity function changes most rapidly in the ultraviolet. Over the range  $\lambda\lambda 3500$  to  $5200$  the rate of change

TABLE II  
OBSERVED RELATIVE CHANGE OF INSTRUMENTAL SENSITIVITY FUNCTION IN MAGNITUDES PER YEAR

$\lambda$	$\delta \dot{S}(\lambda)$
5150	$-0^m.123$
5000	$-0.088$
4700	$-0.026$
4500	$-0.007$
4200	$+0.055$
4040	$+0.076$
3700	$+0.143$
3600	$+0.167$
3500	$+0.190$

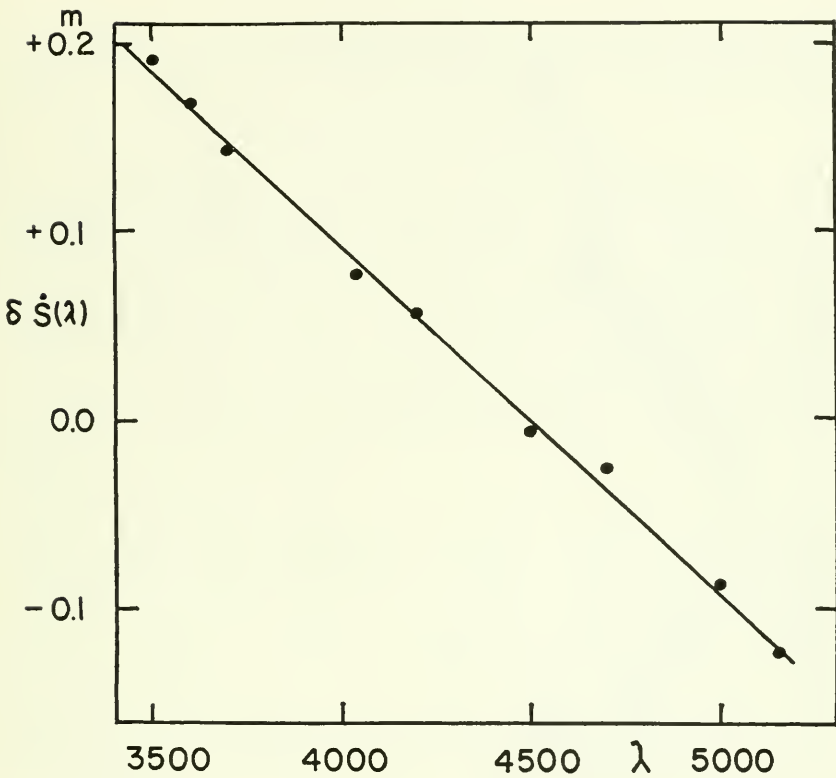


FIG. 2—Rate of change of the instrumental sensitivity function in magnitudes per year, normalized to zero at  $\lambda 4500$ . The rapid decrease of the instrumental sensitivity at short wave-lengths is due to the deterioration of the ultraviolet reflectivity of the mirrors in the light path.

of the sensitivity function in magnitudes per year, at any wave-length relative to that at  $\lambda 4500$  is given by

$$\delta \dot{S}(\lambda) = 1.85 \times 10^{-4} (4500 - \lambda). \quad (2)$$

The fact that the instrumental sensitivity decreases fastest at short wave-lengths is no doubt due to the rapid deterioration of the ultraviolet reflectivity of aluminized reflecting surfaces.

Young (1962) has shown that the spectral response of 1P21 photomultipliers is slightly dependent on temperature. To reduce such temperature-dependent variations of the photomultiplier sensitivity

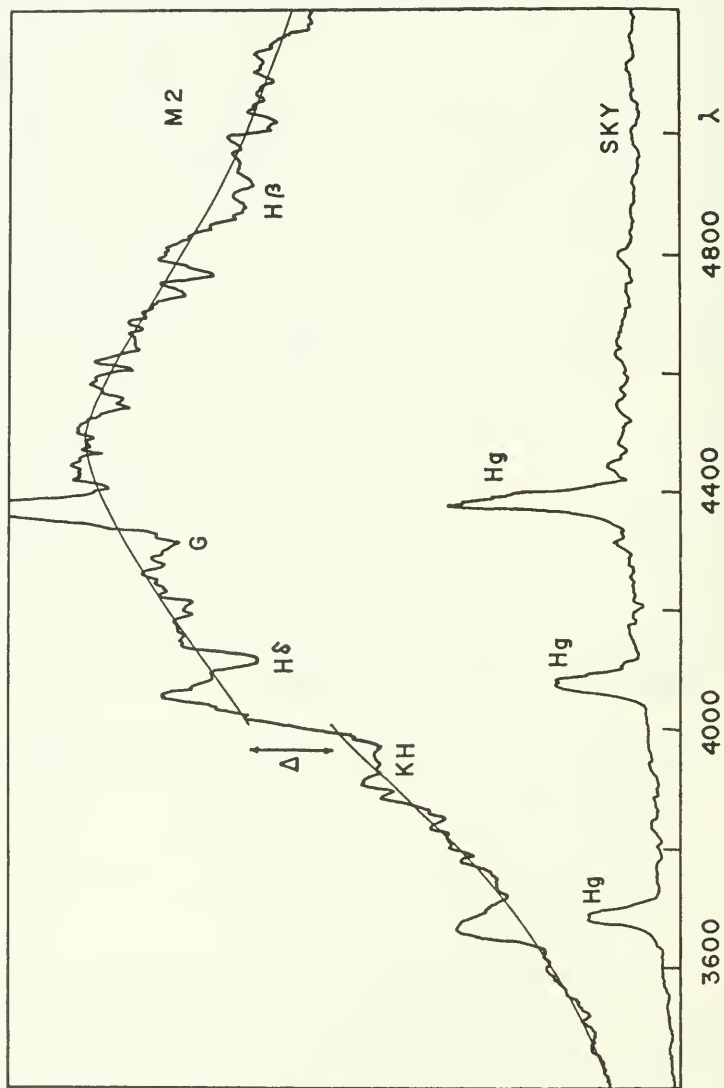


FIG. 3.—Tracing of the globular cluster M2 with sky tracing superimposed. The adopted pseudo-continuum is indicated by the smooth curve.

to a minimum, dry ice was introduced into the cold-box surrounding the 1P21 about one hour before the beginning of the actual observations.

#### REDUCTION OF THE OBSERVATIONS

Figure 3 shows a typical globular cluster tracing with a sky tracing superimposed. The irregular line represents the actually-observed spectral-energy distribution and the smooth curve shows the adopted pseudo-continuum. Except in the regions near  $H\beta$ ,  $H\delta$ , the  $G$ -band and the MgI triplet  $\lambda\lambda 5167-84$  the adopted pseudo-continuum represents the smoothed mean of the actually-observed spectral-energy distribution. Attention should be drawn to the apparent discontinuity in the pseudo-continuum near  $\lambda 4000$ ; just to the red of the  $H\epsilon + H\epsilon$  blend. The size of this discontinuity expressed in magnitudes, will be denoted by the symbol  $\Delta$ .

On each tracing the height of the pseudo-continuum and of the sky background was measured at 100- $\text{\AA}$ . intervals. The intensity difference between sky, and object plus sky, was then converted to a magnitude scale with arbitrary zero point. These magnitudes were then corrected for atmospheric extinction and for the instrumental sensitivity function to yield the absolute energy distribution  $m(1/\lambda)$  at 100- $\text{\AA}$ . intervals. The absolute energy distributions of the same cluster obtained on different nights, each of which contains an arbitrary zero point, were plotted on transparent graph paper and fitted together by visual inspection. The resulting mean absolute energy distributions, normalized to  $m(1/\lambda) = 0.0$  at  $\lambda 4500$ , are given in Table III. A minimum of three tracings on good photometric nights were averaged to obtain the adopted mean absolute energy distribution of a single cluster. (The average number of tracings per cluster was 5.) Also given in Table III are the spectral energy distributions of the galaxies M31 and M32 and of the MK standard stars  $\rho$  Gem (F0 V),  $\beta$  CVn (G0 V) and 61 UMa (G8 V).

The fact that so many globular clusters occur in the general direction of the galactic nucleus necessitated observations down to rather large negative declinations. Many of the clusters contained in the present programme had to be observed through more than two air masses. However, no observations were made at  $\sec z \geq 3.0$ . The fact that so many clusters had to be observed at large values of  $\sec z$  placed very severe demands on the photometric quality of the nights on which

TABLE III  
 ABSOLUTE ENERGY DISTRIBUTIONS OF GLOBULAR CLUSTERS, GALAXIES, AND  
 STANDARD STARS

$\lambda$	NGC 221 (M32)		NGC 224 (M31)		NGC 5024 (M53)	
	n = 6		n = 7		n = 8	
	m(1/ $\lambda$ )	m.e.	m(1/ $\lambda$ )	m.e.	m(1/ $\lambda$ )	m.e.
5200	-0.32	± 0.01	-0.29	± 0.01	-0.30	± 0.02
5100	-0.32	0.01	-0.28	0.01	-0.28	0.01
5000	-0.29	0.01	-0.28	0.01	-0.23	0.01
4900	-0.25	0.01	-0.24	0.01	-0.17	0.01
4800	-0.21	0.01	-0.19	0.01	-0.13	0.01
4700	-0.16	0.01	-0.14	0.01	-0.10	0.01
4600	-0.09	0.01	-0.09	0.01	-0.05	0.01
4500	0.00	0.01	0.00	0.01	0.00	0.01
4400	0.17	0.01	0.20	0.01	0.09	0.01
4300	0.36	0.01	0.42	0.01	0.20	0.01
4200	0.53	0.01	0.62	0.01	0.29	0.02
4100	0.65	0.02	0.75	0.01	0.34	0.02
4000	0.75	0.02	0.82	0.02	0.38	0.03
3900	1.34	0.02	1.57	0.02	0.65	0.04
3800	1.40	0.03	1.65	0.03	0.75	0.04
3700	1.42	0.03	1.66	0.03	0.96	0.06
3600	1.61	0.03	1.79	0.04	1.01	0.08
3500	1.72	0.04	1.89	0.05	1.06	0.09
3400	1.63	0.05	1.89	0.07	1.36	0.12
	NGC 5272 (M3)		NGC 5904 (M5)		NGC 6093 (M80)	
	n = 6		n = 5		n = 3	
$\lambda$	m(1/ $\lambda$ )	m.e.	m(1/ $\lambda$ )	m.e.	m(1/ $\lambda$ )	m.e.
5200	—	—	-0.30	± 0.02	-0.37	± 0.01
5100	-0.27	± 0.02	-0.29	0.01	-0.33	0.01
5000	-0.22	0.01	-0.26	0.01	-0.26	0.01
4900	-0.18	0.01	-0.21	0.01	-0.20	0.01
4800	-0.12	0.01	-0.16	0.01	-0.14	0.01
4700	-0.11	0.01	-0.13	0.01	-0.11	0.01
4600	-0.07	0.01	-0.08	0.01	-0.06	0.01
4500	0.00	0.01	0.00	0.01	0.00	0.01
4400	0.09	0.01	0.07	0.01	0.12	0.02
4300	0.19	0.01	0.19	0.01	0.24	0.02
4200	0.28	0.01	0.28	0.01	0.33	0.02
4100	0.36	0.01	0.35	0.01	0.43	0.02
4000	0.39	0.02	0.40	0.01	0.52	0.03
3900	0.66	0.02	0.74	0.02	0.82	0.03
3800	0.74	0.02	0.84	0.02	0.91	0.04
3700	0.91	0.02	0.97	0.02	1.11	0.05
3600	1.07	0.03	1.16	0.03	—	—
3500	1.22	0.04	1.26	0.05	—	—
3400	—	—	1.52	0.07	—	—

TABLE III (Continued)

$\lambda$	NGC 6205 (M13)		NGC 6229 —		NGC 6254 (M10)	
	n = 7		n = 5		n = 4	
	m(1/ $\lambda$ )	m.e.	m(1/ $\lambda$ )	m.e.	m(1/ $\lambda$ )	m.e.
5200	-0.29	$\pm$ 0.02	-0.33	$\pm$ 0.02	-0.44	$\pm$ 0.06
5100	-0.30	0.02	-0.33	0.02	-0.38	0.04
5000	-0.26	0.01	-0.28	0.01	-0.31	0.03
4900	-0.21	0.01	-0.23	0.01	-0.21	0.03
4800	-0.17	0.01	-0.18	0.01	-0.17	0.02
4700	-0.13	0.01	-0.14	0.01	-0.14	0.02
4600	-0.07	0.01	-0.08	0.01	-0.08	0.02
4500	0.00	0.01	0.00	0.01	0.00	0.02
4400	0.10	0.01	0.10	0.01	0.17	0.02
4300	0.20	0.01	0.23	0.01	0.29	0.02
4200	0.29	0.02	0.33	0.01	0.38	0.02
4100	0.36	0.02	0.43	0.01	0.44	0.02
4000	0.43	0.02	0.52	0.02	0.50	0.03
3900	0.72	0.02	0.82	0.02	0.86	0.04
3800	0.78	0.03	0.89	0.02	0.98	0.05
3700	0.98	0.03	0.99	0.02	1.22	0.07
3600	1.10	0.04	1.20	0.02	1.27	0.09
3500	1.25	0.04	1.31	0.03	—	—
3400	1.42	0.05	1.48	0.03	—	—
	NGC 6273 (M19)		NGC 6341 (M92)		NGC 6356 —	
	n = 4		n = 6		n = 4	
$\lambda$	m(1/ $\lambda$ )	m.e.	m(1/ $\lambda$ )	m.e.	m(1/ $\lambda$ )	m.e.
5200	-0.50	$\pm$ 0.02	-0.30	$\pm$ 0.02	-0.52	$\pm$ 0.02
5100	-0.42	0.02	-0.29	0.02	-0.46	0.02
5000	-0.32	0.02	-0.24	0.01	-0.40	0.02
4900	-0.23	0.02	-0.18	0.01	-0.33	0.01
4800	-0.16	0.02	-0.14	0.01	-0.26	0.01
4700	-0.13	0.02	-0.11	0.01	-0.21	0.01
4600	-0.07	0.02	-0.05	0.01	-0.10	0.02
4500	0.00	0.02	0.00	0.01	0.00	0.02
4400	0.11	0.02	0.08	0.01	0.17	0.02
4300	0.26	0.03	0.16	0.01	0.36	0.03
4200	0.41	0.03	0.23	0.01	0.53	0.03
4100	0.50	0.04	0.32	0.01	0.68	0.04
4000	0.55	0.05	0.40	0.02	0.76	0.05
3900	0.98	0.06	0.58	0.02	1.34	0.06
3800	1.07	0.08	0.72	0.02	1.42	0.10
3700	1.20	0.13	0.88	0.03	1.58	0.12
3600	—	—	1.05	0.04	—	—
3500	—	—	1.20	0.04	—	—
3400	—	—	1.39	0.07	—	—

TABLE III (Continued)

$\lambda$	NGC 6402 (M14)		NGC 6626 (M28)		NGC 6656 (M22)	
	n = 5		n = 5		n = 4	
	m(1/ $\lambda$ )	m.e.	m(1/ $\lambda$ )	m.e.	m(1/ $\lambda$ )	m.e.
5200	-0.67	$\pm$ 0.01	-0.51	$\pm$ 0.03	-0.49	$\pm$ 0.03
5100	-0.56	0.01	-0.44	0.02	-0.45	0.03
5000	-0.44	0.01	-0.36	0.02	-0.37	0.02
4900	-0.33	0.01	-0.28	0.02	-0.27	0.02
4800	-0.25	0.01	-0.22	0.01	-0.22	0.02
4700	-0.18	0.01	-0.18	0.01	-0.19	0.02
4600	-0.10	0.01	-0.11	0.01	-0.10	0.02
4500	0.00	0.01	0.00	0.01	0.00	0.02
4400	0.12	0.01	0.16	0.01	0.08	0.02
4300	0.31	0.01	0.36	0.01	0.21	0.02
4200	0.44	0.02	0.50	0.02	0.33	0.03
4100	0.56	0.02	0.61	0.02	0.38	0.03
4000	0.67	0.03	0.75	0.03	0.38	0.04
3900	1.08	0.04	1.16	0.06	0.80	0.05
3800	—	—	—	—	0.90	0.06
3700	—	—	—	—	1.00	0.09
3600	—	—	—	—	N.B.—Brightest cluster stars avoided.	
3500	—	—	—	—		
3400	—	—	—	—		
$\lambda$	NGC 6779 (M56)		NGC 6838 (M71)		NGC 6865 (M75)	
	n = 5		n = 6		n = 5	
	m(1/ $\lambda$ )	m.e.	m(1/ $\lambda$ )	m.e.	m(1/ $\lambda$ )	m.e.
5200	-0.46	$\pm$ 0.02	-0.48	$\pm$ 0.02	-0.38	$\pm$ 0.03
5100	-0.41	0.02	-0.46	0.02	-0.35	0.02
5000	-0.32	0.02	-0.39	0.01	-0.32	0.02
4900	-0.25	0.01	-0.32	0.01	-0.26	0.02
4800	-0.19	0.01	-0.25	0.01	-0.22	0.01
4700	-0.15	0.01	-0.20	0.01	-0.15	0.02
4600	-0.08	0.01	-0.15	0.01	-0.07	0.02
4500	0.00	0.01	0.00	0.02	0.00	0.02
4400	0.10	0.02	0.19	0.02	0.14	0.02
4300	0.21	0.02	0.40	0.02	0.26	0.02
4200	0.30	0.02	0.53	0.02	0.35	0.03
4100	0.41	0.02	0.63	0.03	0.44	0.03
4000	0.49	0.03	0.69	0.04	0.47	0.04
3900	0.74	0.03	1.34	0.05	0.96	0.05
3800	0.88	0.04	1.30	0.08	1.10	0.06
3700	1.10	0.06	1.36	0.13	1.16	0.10
3600	1.33	0.07	—	—	—	—
3500	1.48	0.10	—	—	—	—
3400	—	—	—	—	—	—

TABLE III (Continued)

$\lambda$	NGC 6934 —		NGC 7006 —		NGC 7078 (M15)	
	n = 4		n = 4		n = 5	
	m(1/ $\lambda$ )	m.e.	m(1/ $\lambda$ )	m.e.	m(1/ $\lambda$ )	m.e.
5200	-0.38	± 0.02	-0.34	± 0.02	-0.29	± 0.02
5100	-0.33	0.02	-0.28	0.02	-0.29	0.02
5000	-0.27	0.02	-0.23	0.02	-0.24	0.01
4900	-0.22	0.02	-0.17	0.02	-0.17	0.01
4800	-0.17	0.01	-0.13	0.02	-0.14	0.01
4700	-0.12	0.01	-0.09	0.02	-0.11	0.01
4600	-0.07	0.01	-0.05	0.02	-0.06	0.01
4500	0.00	0.01	0.00	0.02	0.00	0.01
4400	0.10	0.02	0.08	0.02	0.07	0.01
4300	0.22	0.02	0.19	0.02	0.16	0.01
4200	0.32	0.02	0.26	0.02	0.25	0.01
4100	0.41	0.02	0.34	0.02	0.32	0.01
4000	0.50	0.02	0.41	0.03	0.38	0.01
3900	0.82	0.02	0.75	0.03	0.61	0.01
3800	0.91	0.03	0.80	0.03	0.72	0.01
3700	1.05	0.03	0.91	0.04	0.90	0.02
3600	1.34	0.05	1.08	0.05	1.09	0.02
3500	—	—	1.20	0.08	1.18	0.03
3400	—	—	1.29	0.16	1.30	0.05
	NGC 7089 (M2)		NGC 7099 (M30)			
	n = 5		n = 6			
$\lambda$	m(1/ $\lambda$ )	m.e.	m(1/ $\lambda$ )	m.e.		
5200	-0.29	± 0.04	-0.28	± 0.03		
5100	-0.26	0.02	-0.23	0.02		
5000	-0.21	0.02	-0.17	0.02		
4900	-0.17	0.02	-0.13	0.02		
4800	-0.14	0.01	-0.10	0.02		
4700	-0.11	0.01	-0.08	0.01		
4600	-0.07	0.01	-0.04	0.01		
4500	0.00	0.01	0.00	0.02		
4400	0.10	0.01	0.08	0.02		
4300	0.19	0.01	0.18	0.02		
4200	0.26	0.01	0.25	0.02		
4100	0.33	0.01	0.33	0.02		
4000	0.39	0.01	0.40	0.02		
3900	0.70	0.01	0.62	0.02		
3800	0.78	0.02	0.78	0.03		
3700	0.95	0.02	0.96	0.04		
3600	1.13	0.02	—	—		
3500	1.19	0.03	—	—		
3400	1.28	0.05	—	—		

TABLE III (Continued)

$\lambda$	$\rho$ Gem F0 V		$\beta$ CVn G0 V		61 UMa GS V	
	n = 4		n = 4		n = 4	
	m(1/ $\lambda$ )	m.e.	m(1/ $\lambda$ )	m.e.	m(1/ $\lambda$ )	m.e.
5200	-0.03	$\pm$ 0.01	-0.20	$\pm$ 0.01	-0.24	$\pm$ 0.01
5100	-0.07	0.01	-0.19	0.01	-0.24	0.01
5000	-0.04	0.01	-0.16	0.01	-0.20	0.01
4900	-0.02	0.01	-0.13	0.01	-0.18	0.01
4800	-0.02	0.01	-0.12	0.01	-0.15	0.01
4700	-0.04	0.01	-0.08	0.01	-0.12	0.01
4600	-0.02	0.01	-0.06	0.01	-0.08	0.01
4500	0.00	0.01	0.00	0.01	0.00	0.01
4400	0.04	0.01	0.11	0.01	0.15	0.01
4300	0.07	0.01	0.20	0.01	0.28	0.01
4200	0.12	0.01	0.29	0.01	0.39	0.01
4100	0.17	0.01	0.37	0.01	0.49	0.01
4000	0.22	0.01	0.44	0.01	0.58	0.01
3900	0.48	0.01	0.84	0.01	1.10	0.01
3800	0.63	0.01	0.88	0.01	1.15	0.01
3700	0.93	0.01	0.92	0.01	1.19	0.01
3600	1.05	0.01	1.03	0.01	1.28	0.01
3500	1.15	0.01	1.14	0.02	1.40	0.01
3400	1.24	0.02	1.27	0.02	1.49	0.02

observations were made. In fact many tracings had to be rejected because observations of standard stars showed that some nights were not of the highest photometric quality. Other reasons for rejecting tracings were moderate or strong auroral activity, cloud danger to individual tracings and occasional instrumental difficulties. In the final analysis about one third of all tracings obtained had to be rejected for one of the reasons listed above.

Inspection of Table III shows that absolute energy distributions could not be obtained for all clusters to the extreme short wave-length limit of  $\lambda 3400$ . This was due to the fact that, for globular cluster observations, the difference between total brightness and sky brightness is much smaller in the ultraviolet than it is in the blue-green region of the spectrum. In no cases were differences of less than 0.5 inches between total signal and sky background measured on the tracings.

Inspection of the sample tracing illustrated in figure 3 shows that three wave-length regions, with a width of about 50 A. each, are completely obscured by mercury emission lines of terrestrial origin. Our experience indicates that these lines introduce very little uncer-

tainty in the interpolated position of the pseudo-continuum. In fact these lines were found to furnish convenient wave-length standards for the measurement of the tracings of faint globular clusters. The  $N_2^+$  emission band near  $\lambda 3900$ , which occurs with variable strength during weak aurorae, proved much more bothersome and frequently introduced considerable uncertainty in the measurements of the discontinuity  $\Delta$  near  $\lambda 4000$ .

#### OBSERVATIONAL ERRORS

The mean errors of the absolute energy distribution of globular clusters at each wave-length were estimated from the scatter of the individual observations about the mean. Figure 4 shows a plot of the

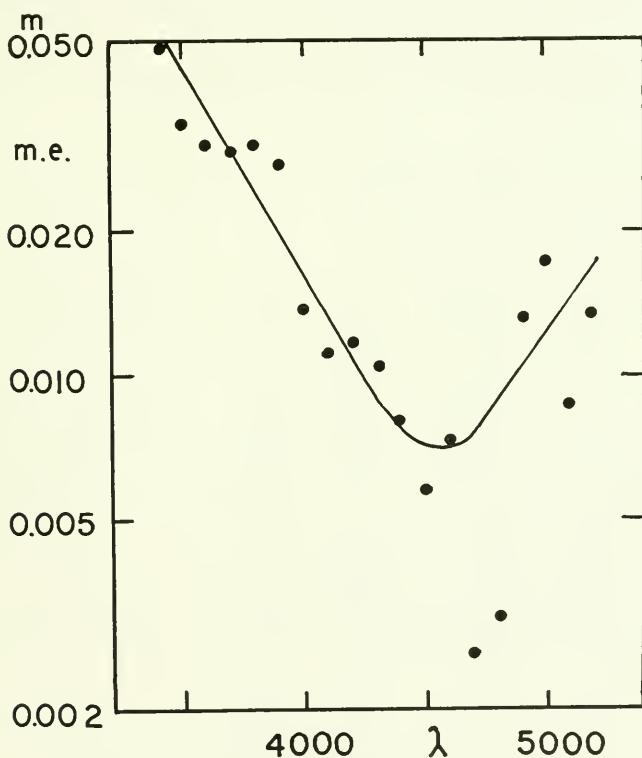


FIG. 4—Wave-length dependence of the observational errors of the absolute energy distribution of M92. The smooth curve shows the adopted wave-length dependence of the errors, the dots the observed errors at each wave-length.

observed mean error of  $m(1/\lambda)$  at each wave-length obtained for M92. The smooth curve in the figure represents the adopted mean error at each wave-length. Comparison of figures 3 and 4 shows that the observational errors are smallest at those wave-lengths at which the observed brightness of globular clusters is greatest. The fact that the extinction corrections are largest in the far ultraviolet probably contributes to the relatively large errors at short wave-lengths. (For  $\sec z = 2.5$  the extinction correction is 1.66 magnitudes larger at  $\lambda 3400$  than it is at  $\lambda 5200$ .) The temperature sensitivity of photomultipliers in the yellow (Young 1962) and the uncertainty of the adopted pseudo-continuum level due to the Mg I triplet  $\lambda\lambda 5167-84$  may contribute to the increase of the observational uncertainties longward of  $\lambda 5000$ .

To ensure adequate wave-length resolution the size of the entrance diaphragm of the spectrophotometer had to be rather small. The  $28''$  diaphragm which was used during all globular cluster observations admitted only a small fraction of the total cluster light. The  $P$  magni-

TABLE IV  
COMPARISON OF P-V AND C(41-51)

NGC	M	P <sub>25</sub>	P-V			C(41-51)		
			A.D.	n	m.e.	n		
5024	53	11.2	0.50	0.00	2	0.63	0.03	8
5272	3	10.1	0.56	0.04	3	0.63	0.02	6
5904	5	10.2	0.63	0.01	4	0.64	0.01	5
6093	80	10.1	0.76	0.02	4	0.76	0.02	3
6205	13	10.7	0.57	0.02	6	0.66	0.02	7
6229	—	11.6	0.64	0.01	2	0.76	0.02	5
6254	10	12.0	0.79	0.01	3	0.82	0.04	4
6273	19	11.2	0.90	0.03	4	0.91	0.05	4
6341	92	9.7	0.53	0.00	2	0.61	0.02	6
6356	—	12.0	1.06	0.02	3	1.13	0.04	4
6402	14	12.9	1.12	0.04	5	1.12	0.02	5
6626	28	—	0.97	0.02	3	1.05	0.03	5
6656	22	11.4	0.86	0.01	2	(0.83)	0.04	4
6779	56	12.8	0.74	0.04	3	0.82	0.03	5
6838	71	13.1	0.95	0.01	2	1.10	0.04	6
6864	75	10.6	0.71	0.00	2	0.79	0.04	5
6934	—	11.4	0.62	0.01	3	0.75	0.02	4
7006	—	12.6	0.61	0.01	2	0.62	0.03	4
7078	15	9.2	0.59	0.01	2	0.61	0.02	5
7089	2	10.1	0.57	0.01	2	0.59	0.03	5
7099	30	10.6	0.48	0.00	2	0.56	0.03	6

tudes of a region with a diameter of  $28''$  centred on the cluster were extrapolated from data given by Kron and Mayall and are given under the column heading  $P_{28}$  in Table IV. The table shows that  $P_{28}$  ranges from  $9^m.2$  for the brightest observed cluster to  $13^m.1$  for the faintest cluster. The  $18.5 \text{ \AA}$ . width of the exit slit reduces the effective brightness of the cluster, which is seen by the photomultiplier, by an additional factor of about 4 magnitudes compared to that which would be observed in wide-band photometry. The resulting weakness of the observed signal undoubtedly contributes significantly to the observational errors for the faintest globular clusters.

The determination of the absolute energy distribution of each globular cluster was based on observations during at least two dark runs. Errors in the determination of the sensitivity function for any one dark run will therefore manifest themselves by an increase in the scatter of the individual absolute energy distributions about the mean. Since only one observation of a given globular cluster was obtained on any one night, deviations of the nightly absorption coefficients from the adopted mean absorption coefficient will also show up as scatter of the individual spectral energy distributions about the mean. It is therefore believed that the mean errors of the absolute energy distribution derived from the scatter of the individual observations which are quoted in Table III, represents a realistic appraisal of the actual accuracy of the results. Any errors in the adopted absolute energy distribution of the primary standard star  $\alpha$  Lyrae will of course be reflected in the results.

An additional check on the accuracy of the data may be obtained from intercomparison of the spectral energy distributions of high latitude, and hence presumably little reddened, clusters which according to Kron and Mayall have the same spectral type and which have been assigned to the same metallic line class by Morgan. Such clusters would be expected to have closely similar spectral energy distributions. Figure 5 shows such a comparison for the high latitude clusters M2 and M53. The figure shows that within the accuracy of the data, the absolute spectral energy distributions of these two clusters are identical.

#### COMPARISON WITH WIDE-BAND PHOTOMETRY

Observations of a number of globular clusters on the  $UBV$  system have been published by Johnson (1959). A more extensive series of

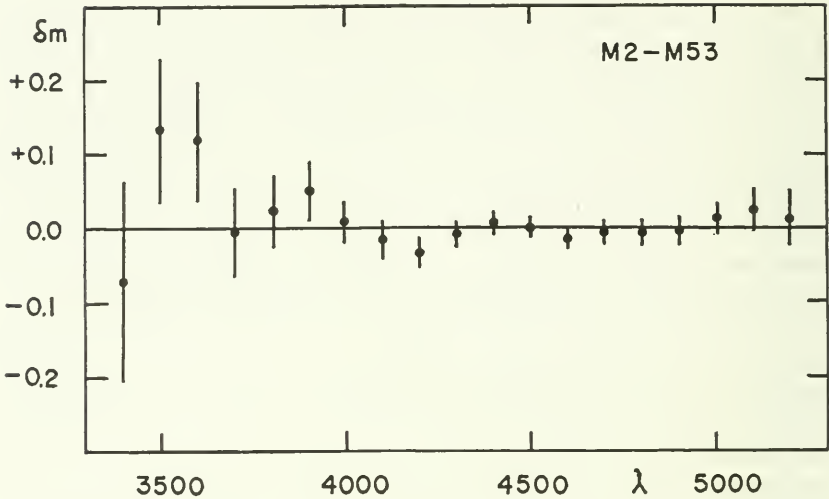


FIG. 5—Observed difference between the absolute energy distributions of the high latitude clusters M2 and M53. Both clusters have the same integrated spectral type and are assigned to the same metallic line strength group by Morgan. The length of the error bars indicates the mean error of each point. Within the accuracy of the data both clusters are seen to have the same absolute energy distribution.

observations on the *PVI* system has been reported by Kron and Mayall (1960). The latter series contains *P-V* colour indices for all of the globular clusters for which absolute energy distributions are given in Table III.

To compare the present results with those of Kron and Mayall it is convenient to introduce monochromatic colour indices. For example, the colour index  $C(41-51)$ , which will be defined as the difference between  $m(1/\lambda)$  at  $\lambda 4100$  and  $m(1/\lambda)$  at  $\lambda 5100$ , may be compared with *P-V*. The observational data on *P-V* and  $C(41-51)$  are listed in Table IV and plotted in figure 6. The figure shows that the data may be adequately represented by the linear relation:

$$C(41-51) = P-V + 0.07. \quad (3)$$

The observations of the very scattered large diameter cluster M22 are not plotted in figure 6. The *P-V* observations of this cluster presumably refer to the integrated light of the entire cluster, whereas individual bright cluster stars had to be avoided during the spectrophotometric observations.

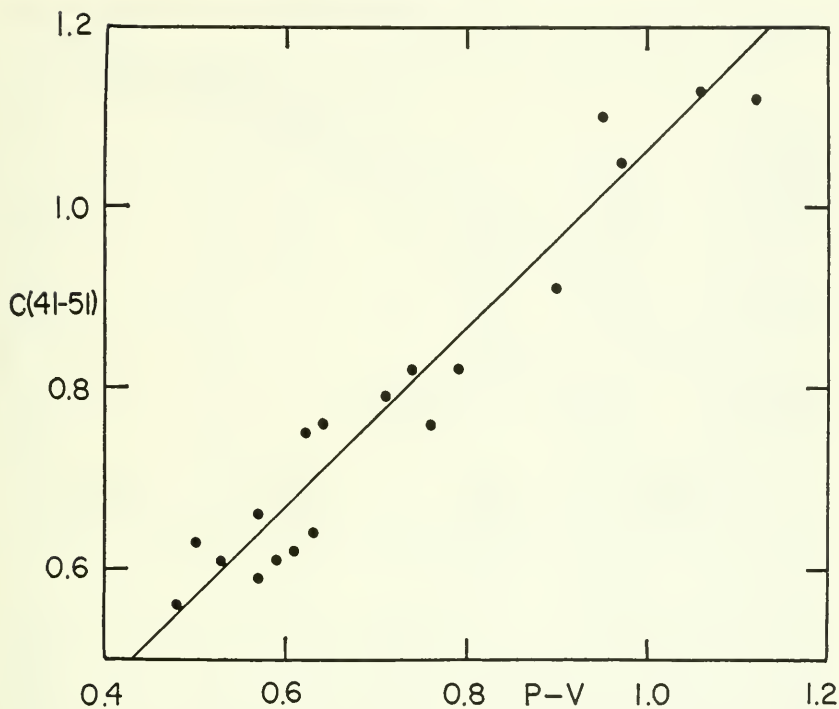


FIG. 6—Comparison of the  $P-V$  colours of globular clusters with the observed monochromatic colour indices  $C(41-51)$ .

Within the accuracy of the data, no systematic differences exist between the  $C(41-51)$  versus  $P-V$  relations for clusters at high and low declinations. Since the low declination clusters were observed through a much larger air mass than the high declination clusters, this provides an additional check on the accuracy of the adopted wave-length dependence of the atmospheric extinction.

#### DISCUSSION OF RESULTS

##### *Intrinsic Differences Between Clusters*

The absolute energy distributions given in Table III for the relatively metal-rich cluster NGC 6356 and for the very metal-poor cluster M92 are compared in figure 7. The figure shows a number of striking differences which cannot be accounted for in terms of differences in the amount of interstellar absorption suffered by these two clusters.

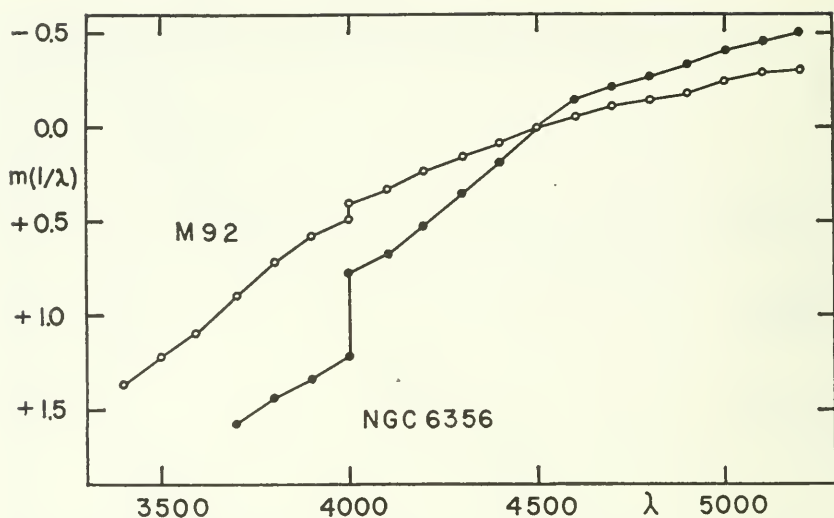


FIG. 7—Comparison of the observed absolute energy distributions of the very metal-poor cluster M92 and the relatively metal-rich cluster NGC 6356.

In the first place figure 7 shows that the discontinuity  $\Delta$  of the adopted pseudo-continuum near  $\lambda 4000$  is very much larger in the metal-rich cluster NGC 6356 than it is in the metal-poor cluster M92. This indicates that the index  $\Delta$  may be correlated with metal abundance. Inspection of the figure also shows that the slope of the pseudo-continuum of the two clusters differs much more strongly over the range  $\lambda\lambda 4100$  to  $4500$  than it does over the range  $\lambda\lambda 4600$  to  $5100$ . This suggests that a combination of the monochromatic colour indices  $C(41-45)$  and  $C(46-51)$  might permit a separation of intrinsic colour effects from the effects of interstellar reddening.

#### *Interstellar Reddening*

In a colour-colour plot using either the *UBV* system (Johnson 1959) or the *PVI* system (Kron and Mayall 1960) the points corresponding to the intrinsic colours of globular clusters lie almost exactly along a reddening line. As a result *UBV* and *PVI* colour observations cannot be used to segregate intrinsic colour effects from the effects of interstellar reddening. Inspection of figure 7 suggests that a two-colour diagram, using the colour indices  $C(41-45)$  versus  $C(46-51)$ , might be useful in separating intrinsic colour effects from interstellar

TABLE V  
MONOCHROMATIC COLOUR INDICES AND PARAMETERS  $\Phi$  AND  $\Psi$

NGC	M	C(41-45) m.e.	C(46-51) m.e.	$\Phi$ m.e.	$\Psi$ m.e.
221	32	0.65±0.02	0.23±0.01	0.47±0.02	1.02±0.03
224	31	0.75 0.02	0.19 0.01	0.60 0.02	1.29 0.02
5024	53	0.34 0.03	0.23 0.02	0.16 0.03	0.37 0.04
5272	3	0.36 0.02	0.20 0.02	0.20 0.02	0.39 0.03
5904	5	0.35 0.01	0.22 0.01	0.18 0.02	0.44 0.02
6093	80	0.43 0.03	0.27 0.02	0.22 0.03	0.49 0.04
6205	13	0.36 0.02	0.23 0.02	0.18 0.02	0.43 0.03
6229	—	0.43 0.02	0.24 0.02	0.24 0.02	0.49 0.03
6254	10	0.44 0.03	0.30 0.04	0.20 0.04	0.47 0.06
6273	19	0.50 0.05	0.35 0.03	0.22 0.05	0.57 0.07
6341	92	0.32 0.01	0.24 0.02	0.13 0.02	0.29 0.03
6356	—	0.68 0.04	0.36 0.02	0.39 0.05	0.88 0.07
6402	14	0.56 0.02	0.46 0.01	0.20 0.03	0.52 0.04
6626	28	0.61 0.03	0.33 0.02	0.35 0.03	0.72 0.07
6656	22	(0.38) 0.04	(0.35) 0.03	(0.10) 0.04	(0.35) 0.06
6779	56	0.41 0.02	0.33 0.02	0.14 0.03	0.33 0.04
6838	71	0.63 0.04	0.32 0.02	0.38 0.04	0.87 0.06
6864	75	0.44 0.04	0.28 0.03	0.22 0.04	0.61 0.06
6934	—	0.41 0.02	0.27 0.02	0.20 0.03	0.48 0.03
7006	—	0.34 0.03	0.23 0.02	0.15 0.04	0.46 0.04
7078	15	0.32 0.01	0.23 0.02	0.14 0.02	0.31 0.02
7089	2	0.33 0.01	0.19 0.03	0.18 0.03	0.44 0.03
7099	30	0.33 0.02	0.19 0.03	0.18 0.03	0.39 0.04
$\rho$ Gem	F0 V	0.17 0.01	0.05 0.01	0.13 0.01	0.41 0.02
$\beta$ CVn	G0 V	0.37 0.01	0.13 0.02	0.26 0.02	0.65 0.02
61 UMa	G8 V	0.49 0.01	0.16 0.01	0.36 0.01	0.86 0.02

reddening. These colour indices as derived from the data in Table III, are given in Table V. Figure 8 shows a plot of  $C(41-45)$  versus  $C(46-51)$  for those clusters for which Morgan has given metallic line strength classifications. Also shown is the reddening line derived from Whitford's (1958) reddening law. The figure shows that metal-rich clusters lie well to the right of the reddening line for metal-poor clusters. The position of a globular cluster in figure 8 may be used to estimate both the metallic line strength classification of that cluster and the reddening of that cluster relative to other clusters of the same metallic line strength. However, the total reddening of the cluster can be

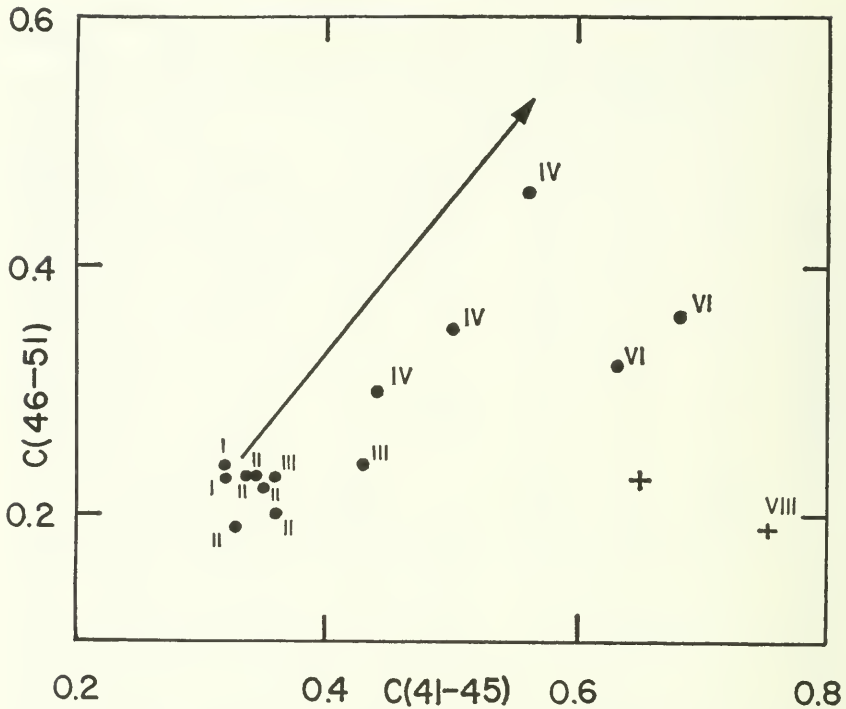


FIG. 8—Two-colour index diagram of globular clusters which have Morgan metallic line strength classifications. The reddening line for metal-poor clusters is indicated by an arrow. The figure shows a clear-cut segregation of intrinsic colour effects from the effects of interstellar reddening. The nuclei of M31 and M32 are indicated by crosses.

determined only after some *a priori* assumption is made about the intrinsic colours of clusters in a certain metallic line strength group.

#### The Metal Abundance Parameter $\Delta$

The size of the discontinuity in the pseudo-continuum near  $\lambda 4000$  was measured directly on each globular cluster tracing (see figure 3). It should be emphasized that such measurements are quite difficult, especially for faint clusters in which the signal-to-noise ratio is small. The strong terrestrial mercury emission lines near  $\lambda 4050$  and the  $N_2^+$  night sky band near  $\lambda 3900$  also contribute to the uncertainty of the measurements. Table VI lists the mean observed values of  $\Delta$ , expressed

TABLE VI  
OBSERVATIONS OF THE DISCONTINUITY  $\Delta$

NGC	M	$\bar{\Delta}$	A.D.	n	Morgan metal class
221	32	0.50	0.04	6	—
224	31	0.59	0.03	5 $\frac{1}{2}$	VIII
5024	53	0.21	0.04	7	II
5272	3	0.20	0.04	9	II
5904	5	0.23	0.03	5	II
6093	80	0.25:	0.11	3 $\frac{1}{2}$	—
6205	13	0.28	0.06	9	III
6229	—	0.20	0.04	6	III
6254	10	0.25:	0.09	2 $\frac{1}{2}$	IV
6273	19	0.40	0.04	4 $\frac{1}{2}$	IV
6341	92	0.09	0.03	9	I
6356	—	0.48	0.05	4	VI
6402	14	0.30	0.03	2 $\frac{1}{2}$	IV
6626	28	0.26:	0.11	4 $\frac{1}{2}$	—
6656	22	(0.31:)	0.08	3	II
6779	56	0.21	0.06	5	—
6838	71	0.52	0.08	8	VI
6864	75	0.26:	0.06	3 $\frac{1}{2}$	—
6934	—	0.23	0.02	4 $\frac{1}{2}$	—
7006	—	0.33	0.02	4 $\frac{1}{2}$	II
7078	15	0.14	0.03	10	I
7089	2	0.23	0.04	5	II
7099	30	0.12	0.04	6	—

in magnitudes, for all the programme clusters. Also given are the average deviation, *A.D.*, of the individual  $\Delta$  observations from the mean and the number of observations, *n*, on which this mean is based. In forming the mean, half weight was given to those  $\Delta$  determinations which were considered to be of lesser accuracy; either because of small deflections on the tracings or on account of the strength of  $N_2^+$  night sky emission. It will be seen that for some clusters the number of observations used to determine  $\Delta$  was larger than the number employed to derive the absolute energy distribution of that same cluster. This is due to the fact that the index  $\Delta$  could be measured on a number of tracings obtained on nights which were not of the highest photometric quality.

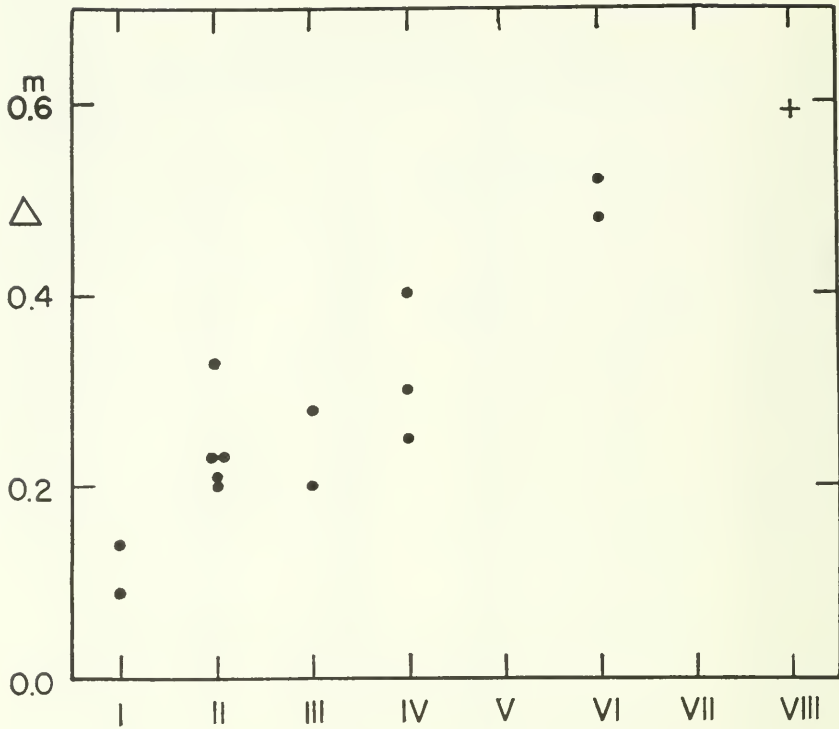


FIG. 9—Correlation between Morgan's metallic line strength classification and the discontinuity  $\Delta$  near  $\lambda 4000$ . The cross represents the nucleus of M31.

For those clusters for which this information is available the metallic line-strength classification (Morgan 1959) is also given in Table VI. Figure 9 shows that the discontinuity index  $\Delta$  correlates well with Morgan's metallic line-strength classification. That such a correlation between metallic line-strength and discontinuity of the observed pseudo-continuum near  $\lambda 4000$  is to be expected may be seen from figure 1 of Wildey *et al.* (1962). Their figure shows that, for F- and G-type stars, the fraction of the radiant flux which is blocked by Fraunhofer lines is much larger to the blue of  $\lambda 4000$  than it is redward of this wave-length.

Additional confirmation of the relation between the size of the  $\Delta$  index and metal abundance is provided by observations (van den Bergh, unpublished) of the  $\Delta$  index in main-sequence stars of differ-

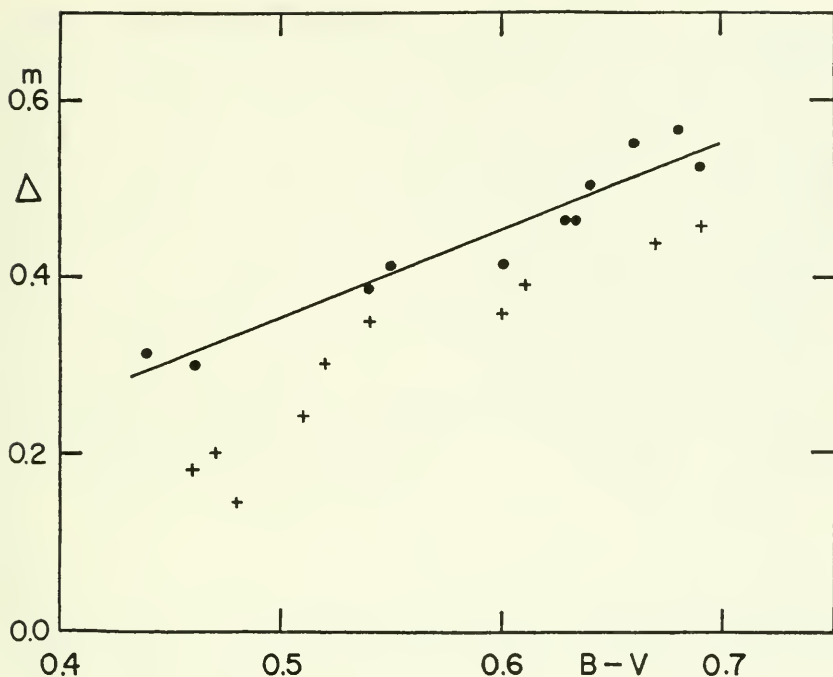


FIG. 10—The figure shows the relation between  $\Delta$  and  $B-V$  for main sequence stars of normal metal abundance (dots) and metal-poor stars (crosses). At a given colour the discontinuity  $\Delta$  is seen to be smaller for metal-deficient stars than for stars of normal metal abundance. The mean relation for stars with normal metal abundances is indicated by a straight line.

ing metal abundances. For these measurements the effective spectral resolution was comparable to that employed during the globular cluster observations. The results of these measurements are plotted in figure 10. The figure shows that, for any  $B-V$  value, stars of normal metal abundance [ $\delta(U-B) < 0.06$ ] have a larger  $\Delta$  value than do metal-poor stars [ $\delta(U-B) > 0.12$ ]. The smallest observed  $\Delta$  value occurs for the subdwarf H.D. 140283, which is the most metal-deficient dwarf star known.

Some caution should be exercised in the interpretation of the relation between metal abundance and the quantity  $\Delta$  in the nuclei of M31 and M32. For composite stellar systems the observed value of  $\Delta$  will depend on both the metal abundance and the frequency

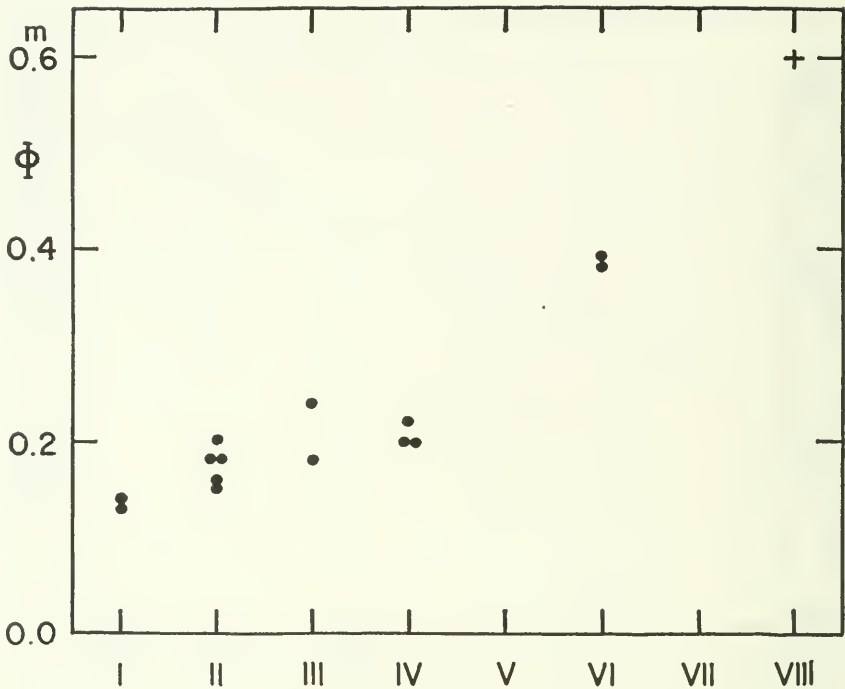


FIG. 11—Relation between the parameter  $\Phi$  and Morgan's metallic line strength classification. The cross represents the nucleus of M31.

distribution of stars in different regions of the colour-magnitude diagram. For example the large value of  $\Delta$  observed for the nucleus of M31 might be due either to a metal-rich stellar population or to a strong contribution of late-type stars to the total light. Also K-type giant stars have larger  $\Delta$  values than do main sequence stars of the same spectral type.

#### *Other Intrinsic Parameters of Globular Clusters*

Using the wave-length dependence of interstellar reddening, which has been determined by Whitford (1958), it is possible to form combinations of monochromatic colour indices which are independent of interstellar reddening. Such reddening-free indices may be regarded as intrinsic parameters of composite stellar systems. For example one may define a quantity

$$\Phi = C(41-45) - 0.8C(46-51), \quad (4)$$

which is a function of the gradient of the absolute energy distribution to the red of the discontinuity  $\Delta$  near  $\lambda 4000$ . The  $\Phi$  indices for all clusters observed during the present programme are listed in Table V. Figure 11 shows that the index  $\Phi$  correlates well with Morgan's (1959) metallic line strength classification. From an observational point of view the index  $\Phi$  has the advantage that it is determined in the blue-green region of the spectrum where the signal-to-sky ratio is large and where atmospheric extinction corrections are not as great as they are in the ultraviolet. Spectrophotometric observations of high- and low-velocity main sequence stars by Greig (1962) also show that combinations of monochromatic colour indices determined in the range  $4100 \leq \lambda \leq 5100 \text{ \AA}$ . yield parameters which correlate with the ultraviolet excess and metal abundance of those stars.

Another reddening-free parameter, which includes the discontinuity  $\Delta$  near  $\lambda 4000$ , may be defined by

$$\Psi = C(39-45) - C(45-51). \quad (5)$$

Due to the inclusion of a measurement in the violet region of the spectrum, the errors associated with the determination of  $\Psi$  are larger than those associated with the measurement of  $\Phi$ . These larger errors are, however, compensated for by the fact that among globular clusters  $\Psi$ , which includes the discontinuity  $\Delta$ , exhibits a wider range of variation than does  $\Phi$ . The values of  $\Psi$  derived from the observations are given in Table V. Figure 12 shows that the parameter  $\Psi$  correlates well with Morgan's metallic line strength classification.

The correlations of  $\Delta$ ,  $\Phi$ , and  $\Psi$  with the integrated spectral types of globular clusters (Kron and Mayall 1960) show considerably more scatter than do the correlations with Morgan's metallic line strength classification. Presumably this indicates that metallic line strength is a more accurate classification parameter than is "integrated spectral type".

The fact that  $\Delta$ ,  $\Phi$ ,  $\Psi$  and metallic line strength classification all correlate well together suggests that they all measure essentially the same parameter i.e. metal abundance. This view receives support from a comparison of the spectral energy distributions of the very metal-poor cluster M92 and the relatively metal-rich cluster NGC 6356. The difference in the visual absorption suffered by these two clusters is  $0^m.7$  for Kron and Mayall's "Solution I" and  $1^m.3$  for their "Solution II". Adopting a visual absorption of  $1^m.0$  and Whitford's reddening law the difference between the true absolute energy distributions of

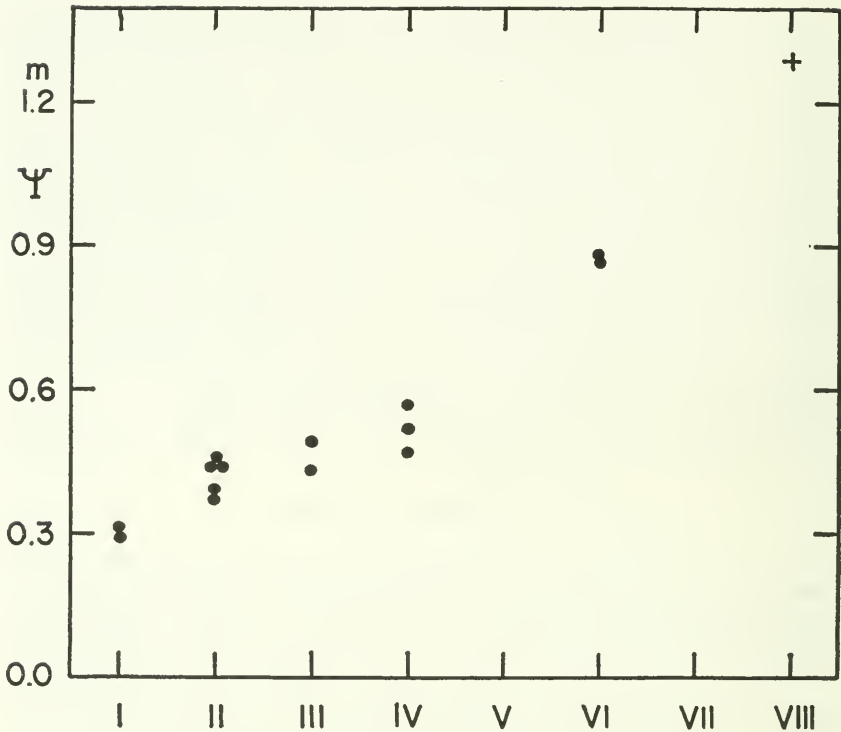


FIG. 12—Relation between the parameter  $\Psi$  and Morgan's metallic line strength classification. The cross represents the nucleus of M31.

these two clusters may be determined. The resulting differences between the absolute energy distributions of M92 and NGC 6356, normalized to zero at  $\lambda 4500$ , are plotted in figure 13. Also shown in the figure 13 is the quantity  $\epsilon_{\lambda}$ ; the fraction of the total energy in the solar continuum (Michard 1950) which is blocked by Fraunhofer lines. The similarity of these two curves strongly suggests that differences between the metal abundances of the stars in M92 and NGC 6356 are largely responsible for the observed differences of the absolute energy distributions of these two clusters.

#### *Comparison of M31 and M32 with Globular Clusters*

In Table VII the indices  $\Delta$ ,  $\Phi$ , and  $\Psi$  for the nuclei of the galaxies M31 and M32 are compared with those of the relatively metal-rich

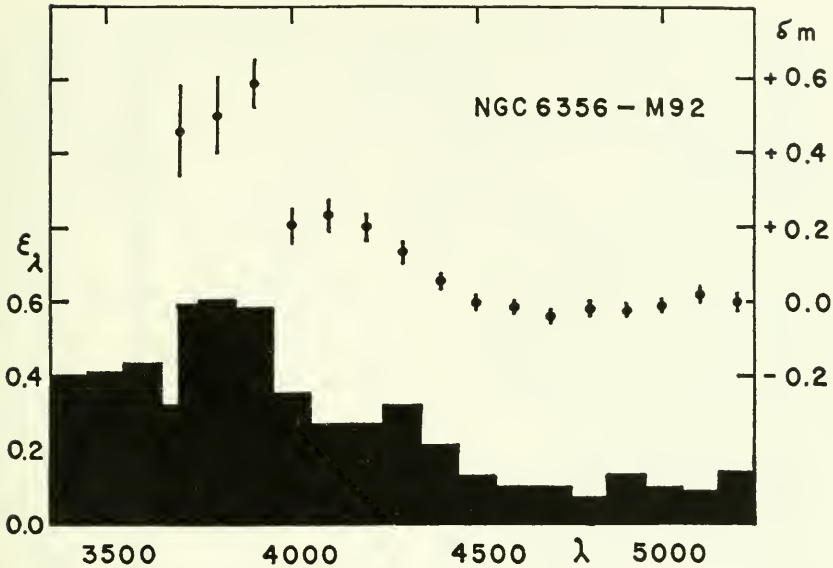


FIG. 13—Difference between the true absolute energy distributions of the relatively metal-rich cluster NGC 6356 and the very metal-poor cluster M92 under the assumption that the interstellar absorption  $A_v$  suffered by NGC 6356 is 1.0 magnitudes larger than that suffered by M92. Error bars indicate means errors of each difference. The histogram shows the fractional blocking of radiant energy by Fraunhofer lines in the sun. The similarity of the two curves suggests that the observed differences between the spectral energy distributions of the two clusters may be largely accounted for by the difference in their metal abundances.

TABLE VII  
COMPARISON OF M31, M32 AND GLOBULAR CLUSTERS

	$\bar{\Delta}$	$\Phi$	$\Psi$	Morgan metal class
M31	0.59	$0.60 \pm 0.02$	$1.29 \pm 0.02$	VIII
M32	0.50	$0.47 \pm 0.02$	$1.02 \pm 0.03$	—
NGC 6356	0.48	$0.39 \pm 0.05$	$0.88 \pm 0.07$	VI
M71	0.52	$0.38 \pm 0.04$	$0.87 \pm 0.06$	VI

globular clusters NGC 6356 and M71. The data in the table show that, for the nucleus of M31, the indices  $\Delta$ ,  $\Phi$ , and  $\Psi$  are larger than those observed for the two least metal-deficient clusters observed during the present programme. The parameters  $\Delta$ ,  $\Phi$ , and  $\Psi$  for the

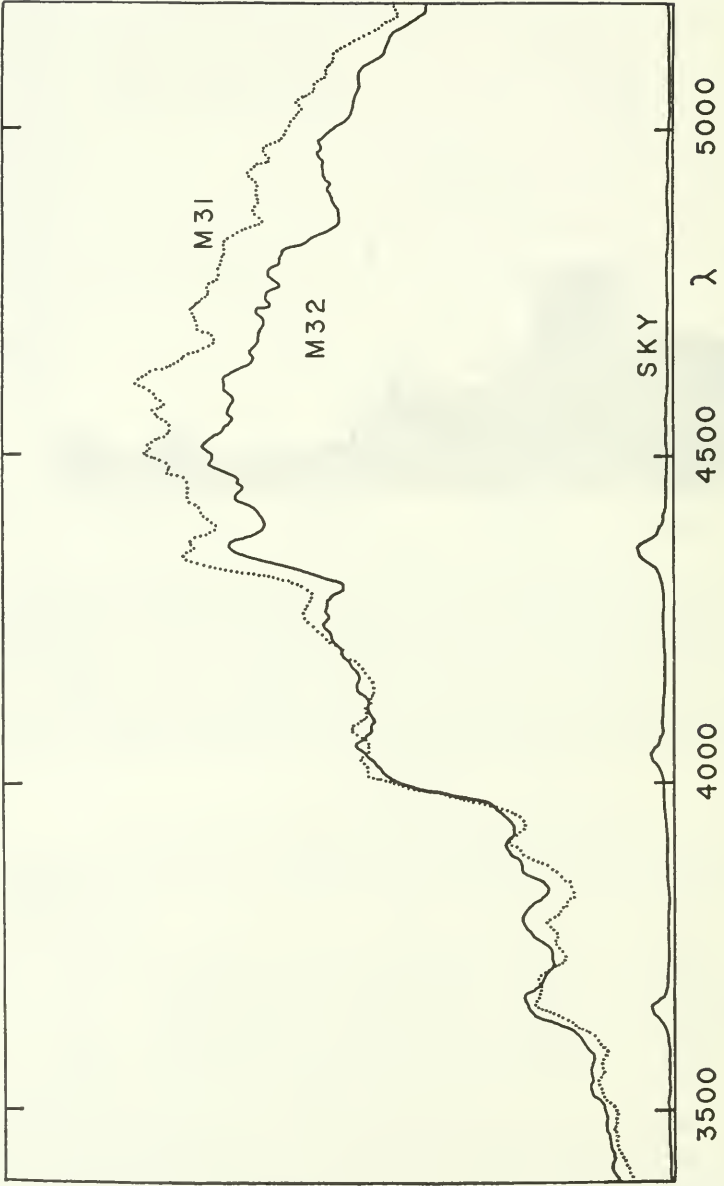


FIG. 14—Comparison of tracings of the nuclei of M31 and M32 with sky tracing superimposed. The figure shows that M32 is bluer than M31.

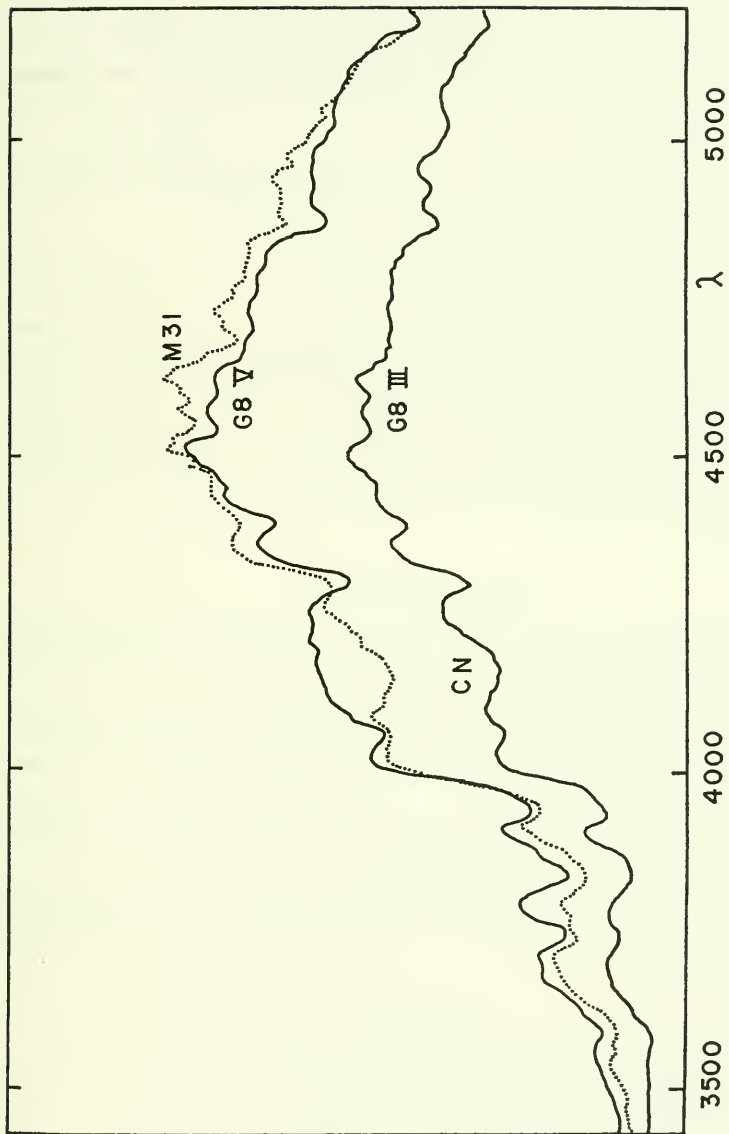


FIG. 15—Comparison of a tracing of M31 (with sky subtracted) with tracings of the stars  $\eta$  Psc (G8 III) and  $\delta$  UMa (G8 V). The strength of the cyanogen absorption in the tracing of M31 shows that giant stars contribute significantly to the total luminosity of the nucleus of M31 in blue light.

nucleus of M32 appear to be intermediate between those of M31 and those of the least metal-deficient globular clusters observed. Morgan (1959) lists four globular clusters which he considers to be metal-richer than M71 and NGC 6356. Unfortunately these clusters were either too far south or too faint to be observed during the present programme.

Figure 14 shows tracings of M31 and M32 obtained on the same night and at the same value of sec  $z$ . Comparison of these two tracings shows that M32 is considerably bluer than is M31.

Figure 15 shows a comparison of a tracing of M31 with tracings of a G8 III giant and a G8 V dwarf. For the scans of the two stars the width of the exit slot was increased to make the effective resolution similar to that on the tracing of M31. Comparison of the three tracings in the region between  $\lambda\lambda 4100$  and  $4200$  shows that "cyanogen giants" must provide a major contribution to the total radiation of the nucleus of M31 in the blue region of the spectrum. Morgan and Mayall (1957) have arrived at the same conclusion from an examination of low dispersion spectra of M31.

#### ACKNOWLEDGMENTS

We are deeply indebted to Dr. John F. Heard for making large blocks of 74-inch telescope observing time available to us during the summers of 1961 and 1962.

Thanks are also due to Mr. W. E. Greig for occasional assistance at the telescope and to Mr. W. H. Clarke for advice on the computer reduction of the observations.

One of us (R.C.H.) wishes to acknowledge the receipt of the 1961-1962 Chant Fellowship in Astronomy.

Part of this work was supported by grants from the Advisory Committee on Scientific Research, Toronto, and the National Research Council, Ottawa.

#### REFERENCES

- Bless, R. C. 1958, Univ. of Michigan Ph.D. Dissertation.  
Greig, W. E. 1962, Univ. of Toronto, M.A. Thesis.  
Johnson, H. L. 1959, *Lowell Obs. Bull.*, vol. 4, p. 117.  
Kinman, T. D. 1959, *R.A.S., M.N.*, vol. 119, p. 538.  
Kron, G. E. and Mayall, N. U. 1960, *A. J.*, vol. 65, p. 581.  
Mayall, N. U. 1946, *Ap. J.*, vol. 104, p. 290.

- Michard, R. 1950, *B.A.N.*, vol. 11, p. 227 (no. 416).  
Morgan, W. W. 1956, *P.A.S.P.*, vol. 68, p. 509; 1959, *A.J.*, vol. 64, p. 432.  
Morgan, W. W. and Mayall, N. U. 1957, *P.A.S.P.*, vol. 69, p. 291.  
Oke, J. B. 1960, *Ap. J.*, vol. 131, p. 358.  
Whitford, A. E. 1958, *A.J.*, vol. 63, p. 201.  
Willey, R. L., Burbidge, E. M., Sandage, A. R. and Burbidge, G. R. 1962, *Ap.J.*,  
vol. 135, p. 94.  
Young, A. T. 1962, *A.J.*, vol. 67, p. 286.

